Available online at www.sciencedirect.com
SCIENCE DIRECT®
ELSEVIER
Journal of Nuclear Materials 322 (2003) 195–203
journal of nuclear materials
www.elsevier.com/locate/jnucmat

Microstructural study of hydride formation in Zr–1Nb alloy

S. Neogy, D. Srivastava, R. Tewari, R.N. Singh, G.K. Dey *, S. Banerjee

Materials Science Division, Bhabha Atomic Research Centre, Trombay Mumbai 400 085, India

Received 30 January 2003; accepted 14 July 2003

Abstract

Hydriding of Zr–1Nb alloy having a microstructure comprising equiaxed α grains and a uniform distribution of spherical particles of the β-phase has been carried out in this study. The specimens were hydrided by gaseous charging method to different hydrogen levels. The microstructures of hydrided samples were examined as a function of hydrogen content. The formation of δ-hydride in slow cooled specimens and formation of γ-hydride in rapidly cooled specimens has been studied with their morphology, habit plane and orientation relationship with the α matrix in view. The habit planes of either type of hydride phase has been determined and compared with those observed in other Zr–Nb alloys. The orientation relationship between the α matrix and the δ-hydride was found to be the following: $(0\,0\,0\,1)_\alpha \| (\bar{1}\,1\,\bar{1})_\delta$ and $[1\,1\,\bar{2}\,0]_\alpha \| [1\,1\,0]_\delta$. The orientation relationship between the α matrix and the γ-hydride was of the following type: $(0\,0\,0\,1)_\alpha \| (0\,0\,1)_\gamma$ and $[1\,\bar{2}\,1\,0]_\alpha \| [1\,\bar{1}\,0]_\gamma$. The internal structure of both types of hydride has been examined. The effect of the presence of the spherical β-phase particles in the α matrix on the growth of the hydride plates has been investigated.

1. Introduction

Hydriding of zirconium alloys in reactors has been of great concern, which normally defines the life and performance of various zirconium alloy reactor components in water and steam-cooled nuclear reactors [1]. Although unalloyed zirconium and zirconium-rich alloys dissolve up to 450 ppm hydrogen in solid solution at around 500 °C, the solubility decreases markedly as the temperature is lowered, with 65 ppm hydrogen at 300 °C and 0.05 ppm hydrogen at room temperature [2]. Finished zirconium alloy structural components normally contain 10 ppm of hydrogen [1]. The zirconium-alloy structural components in nuclear reactors absorb hydrogen through various sources, such as moisture present in fuel pellets, hydrogen produced due to radiolysis of water, reaction of zirconium with the coolant water ($Zr + 2H_2O \rightarrow ZrO_2 + 2H_2$) etc. [1,3]. During reactor service, additional hydrogen produced primarily from the corrosion process diffuses into the zirconium-alloy structural components and, when present in quantities above the solubility limit, it precipitates as a brittle zirconium hydride phase [1] which can have three possible crystal structures: γ-hydride (ZrH) with a face-centered tetragonal structure ($c/a > 1$), δ-hydride (ZrH_2) with a face-centered cubic structure, and ε-hydride (ZrH_2) which also has a face-centered tetragonal structure ($c/a < 1$) [4,5]. It is reported that the precipitation of zirconium hydride in zirconium alloys drastically reduces the ductility, fracture toughness and impact strength at room temperature as well as at reactor operating temperatures [2,6]. The degree of embrittlement of zirconium alloy structural components critically depends on the hydride orientation and its morphology [7]. The hydride precipitates have a characteristic acicular or plate morphology, which is often referred to as a 'cornflake' structure [8].

In Russian pressurized water reactors (PWR) of VVER type Zr–1Nb alloy is being used as cladding material [9]. In pressurized heavy water reactors (PHWR) Zr–2.5Nb is used as a pressure tube material [10–12]. These Zr–Nb alloys have shown superior

* Corresponding author. Tel.: +91-2559 5063.
E-mail address: gkdey@apsara.barc.ernet.in (G.K. Dey).

0022-3115/$ - see front matter © 2003 Elsevier B.V. All rights reserved.
doi:10.1016/j.jnucmat.2003.07.002

properties mainly resistance to corrosion and irradiation creep, in comparison to Zircaloys [10,13]. The hydrogen pick up rate in these alloys is also substantially lower [14]. In addition to binary alloys, Zr base ternary and quaternary alloys are being developed for cladding tube application. Some of these are Zr–1Nb–1Sn and Zr–1Nb–1Sn–0.1Fe alloys [15–17]. These alloys have shown much improved in-reactor performance. They have been found to be very useful for higher burn up of the fuel.

In recent studies on zirconium based structural alloys, hydride formation has mainly been studied in Zr–2.5Nb [8,18] and in Zircaloys [2,19,20]. The studies on Zr–2.5Nb or Zr–Nb alloys have shown that the amount of hydride phase and the morphology of hydride precipitated are very sensitive to the morphology and distribution of the β-phase (bcc structure), which has relatively high solubility for hydrogen [8].

Unlike Zircaloys which are mainly single α-phase (hcp structure) material, in Zr–2.5Nb alloy the microstructure consists of lamellar arrangement of α-phase with the second phase β distributed as stringers along the grain boundaries of the α-phase [21]. The microstructure of Zr–1Nb alloy is expected to be different from both Zircaloys and Zr–2.5Nb. Hence, it is interesting to investigate the formation of hydride in this alloy and examine the role of β-phase in hydride formation.

The aim of the present study was therefore

(1) to study the formation of various hydride phases in Zr–1Nb alloy and characterize the crystallographic features of these phases;
(2) to decipher the mechanism of hydride formation in Zr–1Nb alloy and compare it with the hydride formation in other zirconium base alloys.

2. Experimental

In the present study hydrogen charging of Zr–1Nb samples were carried out by gaseous hydrogen charging method to different hydrogen levels. Anhydrous zirconium hydride powders in palletized condition were used as the source of hydrogen. For hydrogen charging, the specimens were heated to a temperature varying from 377 to 400 °C. The amount of hydrogen absorbed by the specimen was calculated from the hydrogen pressures shown by the manometer. Before hydrogen charging the surface of the specimens were roughened by grinding with emery papers to increase the surface area for hydrogen absorption.

Two different heat treatment schedules were adopted to produce equilibrium (δ) and metastable (γ)-hydride phases. In the former case after the dissolution treatment at 400 °C the hydrogen charged samples were cooled in the furnace to the room temperature (slow cooled, heat treatment A) and in the later case the samples were rapidly cooled by quenching in water (rapidly cooled, heat treatment B).

The etchant used to develop microstructures of samples for optical microscopy was having a composition of 50 ml H_2O, 45 ml HNO_3 and 5 ml HF. Specimens for transmission electron microscopy (TEM) were prepared by twinjet electropolishing using an electrolyte consisting of a solution of 80% methanol and 20% perchloric acid at a temperature of −50 °C and using a voltage of 25 V. TEM studies were carried out using JEOL 2000 FX microscope.

3. Results

3.1. Microstructure of as-received Zr–1Nb alloy

A very fine microstructure was observed under the optical microscope in the finished tube of Zr–1Nb alloy. The details of the microstructure could not be resolved at the optical microscope level. Hence further microstructural studies were carried out in TEM. TEM examination of the Zr–1Nb alloy sample exhibited the presence of two-phase microstructure. The matrix phase (α, hcp) was found to be equiaxed in which spherical second phase particles (β, bcc) has been found to be distributed inside as well as at the grain boundaries of the matrix phase (Fig. 1). After examining a large area of several samples in different possible orientations, the size and the size distribution of the two phases were estimated. Typical grain size of the α-phase was found to be in the range of 3–5 μm. The average β particle size were lying in the range of 40–60 nm, the maximum and minimum sizes being 100 and 10 nm respectively. Majority of the particles was in the range of 20–60 nm. Texture analyses of the tube samples were carried out and it was found that majority of the basal poles are lying in the radial direction.

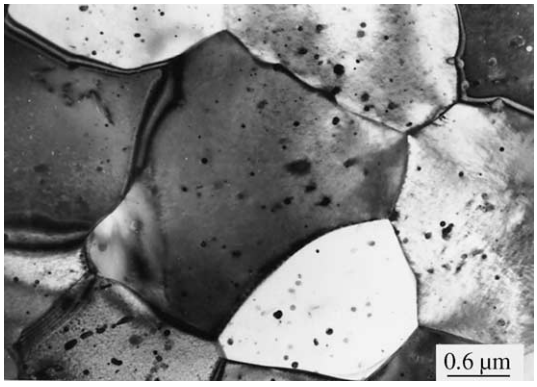

Fig. 1. Bright field TEM micrograph showing the two-phase (α + β) microstructure of as-received Zr–1Nb alloy.

3.2. Microstructure of hydrogen charged Zr–1Nb alloy samples after heat treatment A

The slow cooled hydrogen charged Zr–1Nb alloy samples were examined under optical microscopy as well as under TEM. The important features of hydride formation and its morphology are described in the following sections.

3.2.1. Optical microscopy

Zr–1Nb alloy tube samples were examined in all the three principal directions: axial, radial and circumferential. The hydrides were found to lie in the axial–circumferential plane. The optical micrographs of radial–axial plane of the samples charged with 20, 70 and 140 ppm of hydrogen are shown in Fig. 2(a)–(c) respectively. Typical thread like morphology of the hydrides could be seen. As expected the number density of hydride plates has increased with the increase in hydrogen concentration.

3.2.2. TEM study of hydrogen charged samples

Since the hydride observed in the optical study were very coarse (average size ~20 μm), these coarse hydrides could not be seen under TEM. However, finer hydrides, which were unresolved in the optical microscope, could be easily seen in TEM. It, therefore, can be inferred that the sizes of the hydride plates vary a lot from few microns to tens of microns and hydrides observed under TEM are those hydrides, which formed at the later stage of transformation. These finer hydrides were, however, much smaller in number density. Fig. 3(a) is a typical bright field TEM micrograph, which shows the presence of a hydride plate (marked by an arrow). The hydrides were generally observed to be of acicular shape with sharp interface, a morphology similar to the observed morphology of hydride in several other Zr base alloys. Typical length of this kind of hydride plate was in the range of 1–2 μm and their width was in the range of 0.1–0.2 μm. The aspect ratio was in the range of 5–20. Fig. 3(b) is a microdiffraction pattern obtained from the hydride plate. Analysis of this microdiffraction pattern confirmed that the hydride was the equilibrium δ-hydride (ZrH_2) phase with a face-centered cubic (fcc) structure (lattice parameter $a = 0.478$ nm). The morphology of the δ-hydride plate stated above was noticed in all the samples charged with different hydrogen content viz. 20, 70 and 140 ppm. When the samples were tilted systematically it was observed that the hydride plates were generally associated with dislocations (Fig. 3(c)) indicating the presence of transformation induced strain. In addition to the acicular morphology of the hydride plates, coarse hydride plates with zigzag morphology were also seen in samples charged with 70 and 140 ppm hydrogen. It could be noticed from Fig. 3(d) that the zigzag morphology of the hydride plate maintains its registry while crossing a α grain boundary. A closer examination has shown that the hydride plate with zigzag morphology was made up of stacks of small hydride plates where the individual hydride plates (marked by arrow) building up the stack could be clearly seen in Fig. 3(e). Typical length of this kind of hydride plate was in the range of 2–3 μm and width in the range of 0.4–0.5 μm. The aspect ratio was in the range of 4–7.5. Fig. 3(f) shows a selected area electron diffraction (SAED) pattern taken from this kind of hydride plate confirming it to be the δ-hydride.

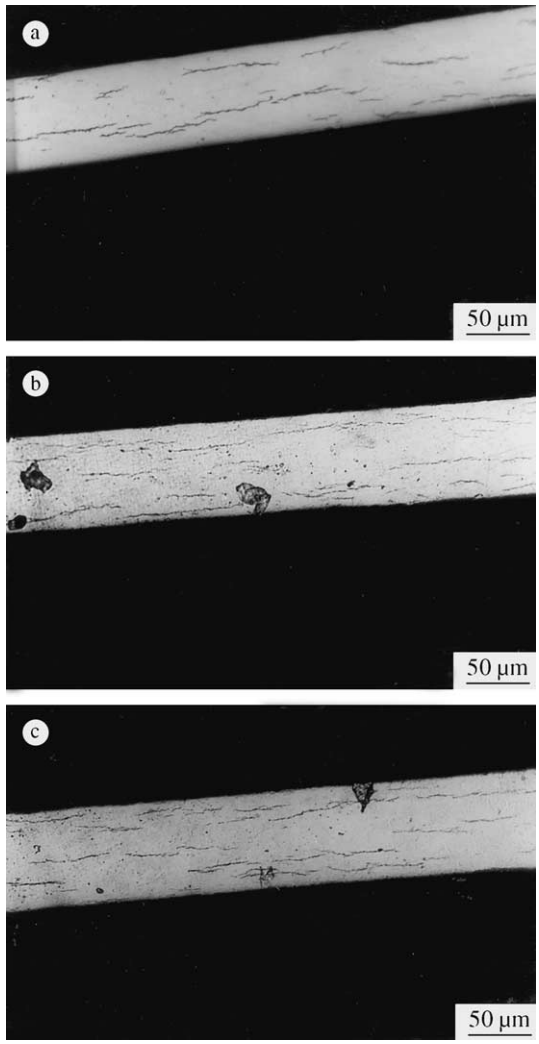

Fig. 2. Optical micrographs showing the δ-hydride plates in the radial–axial plane of the samples (a) 20 ppm, (b) 70 ppm and (c) 140 ppm.

Fig. 3(g) shows the composite SAED pattern containing reflections from both the phases (α + δ). It could be seen from the Fig. 3(g) that the zone axis $[\bar{2}1\,1\,0]$ of the α-phase was nearly parallel to the zone axis $[0\,\bar{1}\,\bar{1}]$ of

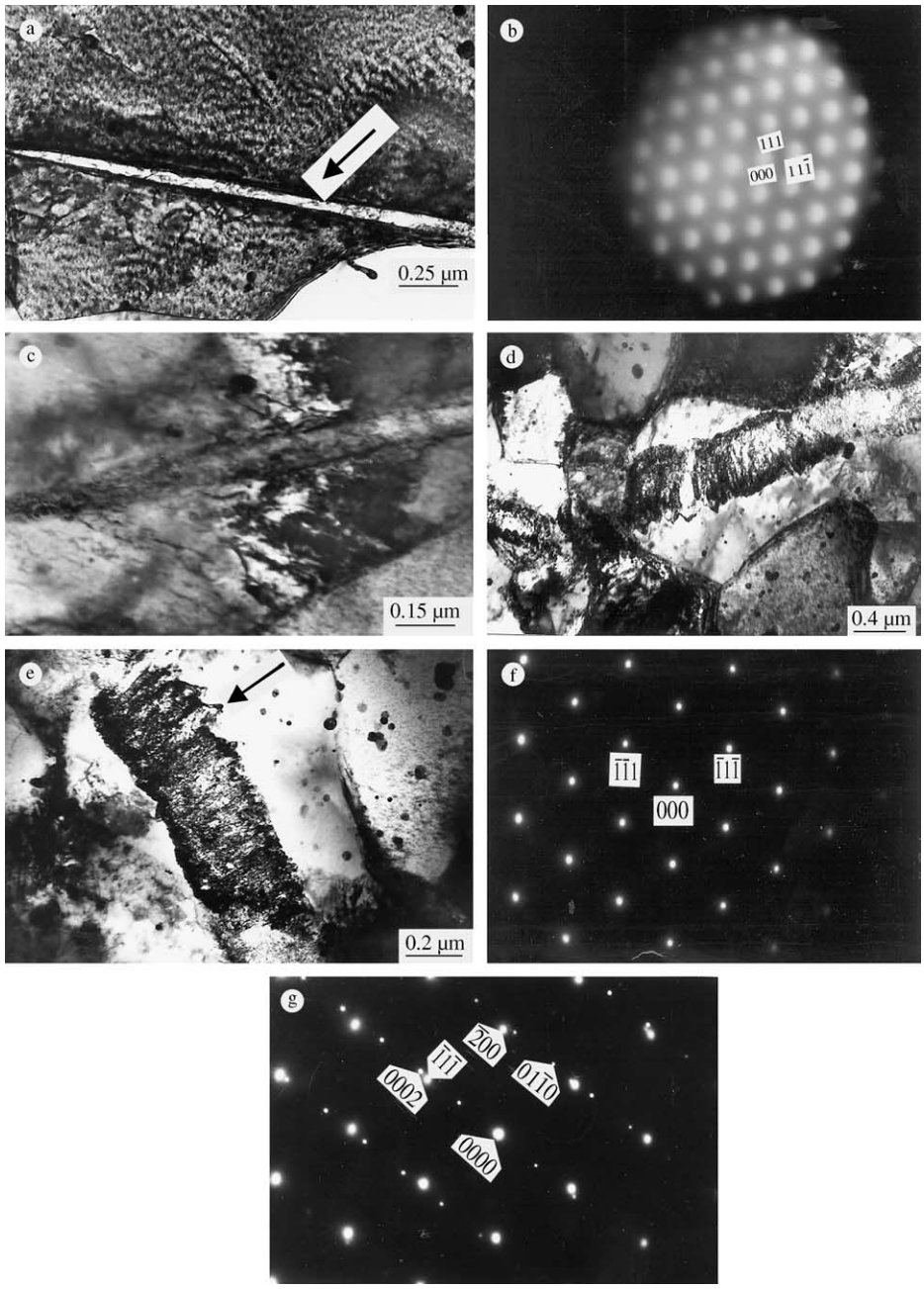

Fig. 3. (a) Bright field TEM micrograph showing the acicular morphology of the δ-hydride plate. (b) Microdiffraction pattern obtained from the δ-hydride plate. Zone Axis = $[1\,\bar{1}\,0]$. (c) Bright field TEM micrograph showing the presence of dislocations around the hydride plate. (d) Bright field TEM micrograph showing the zigzag morphology of the δ-hydride plate. (e) Bright field TEM micrograph showing the individual hydride plates making a large zigzag δ-hydride plate. (f) SAED pattern obtained from the zigzag morphology δ-hydride plate. Zone Axis = $[0\,1\,1]$. (g) Composite SAED pattern showing reflections from α and δ-phases. Zone $\text{Axis}_{\alpha} = [\bar{2}\,1\,0]$ and Zone $\text{Axis}_{\delta} = [0\,\bar{1}\,\bar{1}]$.

the δ-phase and further the $(0\,0\,0\,1)$ plane of α was nearly parallel to $(\bar{1}\,1\,\bar{1})$ plane of δ. This indicates that the orientation relationship (OR) existing between the α and δ-hydride phases, which could be expressed as: $(0\,0\,0\,1)_{\alpha}\|(\bar{1}\,1\,\bar{1})_{\delta}$ and $[1\,1\,\bar{2}\,0]_{\alpha}\|[1\,1\,0]_{\delta}$ is similar to those reported earlier [8,22].

The habit plane determination was carried out for hydride plates with acicular morphology as shown in

Fig. 3(a). Single surface trace analysis method was used to determine the habit plane. The habit planes of the δ-hydride determined in all samples were within 40° from the (0 0 0 1) plane of the α-phase.

3.3. Microstructure of hydrogen charged Zr–1Nb alloy samples after heat treatment B

The formation of hydride in rapidly cooled samples was examined using optical and TEM. The important results are described in the following sections.

3.3.1. Optical microscopy

Typical optical micrographs of samples charged with 20, 70 and 140 ppm of hydrogen is given in Fig. 4(a)–(c), which shows the distribution of hydrides in the radial–axial plane. It could be noticed that upon increasing the hydrogen content the number density of the hydride plates has increased. The morphology of the hydride plates appeared to be similar to those observed in samples treated with heat treatment A.

3.3.2. TEM study of hydrogen charged samples

TEM examination of all the samples charged with different hydrogen content viz. 20, 70 and 140 ppm has revealed needle like morphology of hydrides with sharp interfaces. A typical micrograph of the hydride plate is shown in Fig. 5(a). After examination of many such hydrides in all the samples it was noticed that (i) majority of hydrides are transgranular in nature and (ii) most of these hydrides have originated from the α-phase grain boundaries indicating that the grain boundaries of the α-phase are the preferred sites for nucleation of the hydride plates. In the present study in many instances the γ-hydride plate was found to cut across the β-phase. Typical lengths of these hydrides were found to be in the range of 1.5–2 μm and width in the range of 0.1–0.15 μm. The aspect ratio was in the range of 10–20. The identity of the hydride plates were established using SAED patterns. These patterns could be analyzed in terms of a face-centered tetragonal structure (lattice parameters: $a = 0.4595$ nm and $c = 0.4968$ nm) confirming that the hydride phase formed upon quenching was the γ-hydride. Fig. 5(b) shows the SAED pattern obtained from the $[\bar{1}\,1\,0]$ zone of the γ-hydride plate.

Fig. 5(c) shows the composite SAED pattern consisting of reflections from $[\bar{2}\,4\,\bar{2}\,\bar{3}]$ zone of the α and $[1\,\bar{1}\,\bar{1}]$ zone of the γ-phases. Fig. 5(d) is a key to the SAED pattern shown in Fig. 5(c). The presence of $(\bar{1}\,\bar{1}\,0)$ superlattice reflection (marked by an arrow) which confirms the presence of γ-hydride [23] could be seen in the diffraction pattern of Fig. 5(c). The orientation relationship between the α and the γ lattices appears to be similar to the earlier reported [24]: $(0\,0\,0\,1)_\alpha \| (0\,0\,1)_\gamma$ and $[1\,\bar{2}\,1\,0]_\alpha \| [1\,\bar{1}\,0]_\gamma$.

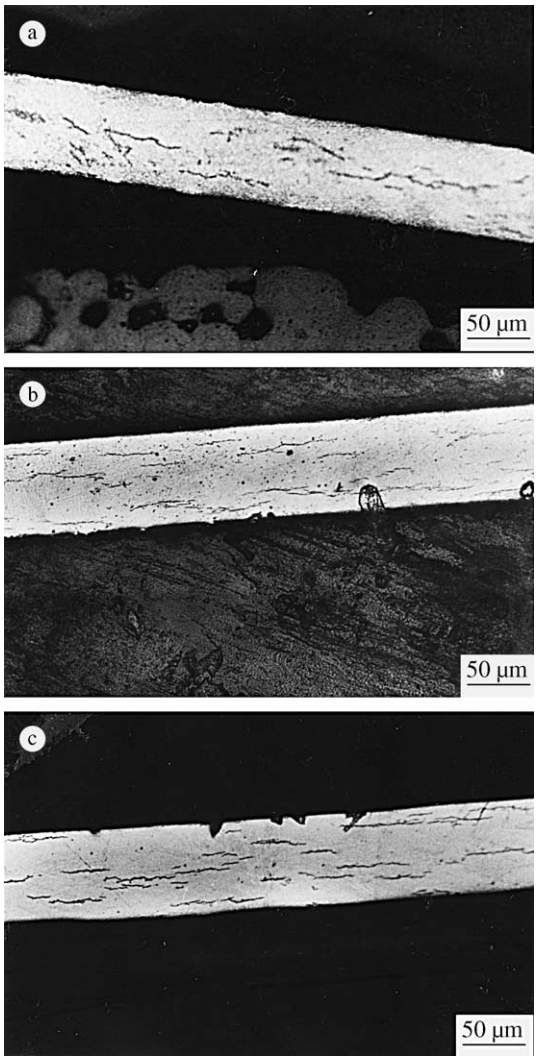

Fig. 4. Optical micrographs showing the γ-hydride plates in the radial–axial plane of the samples (a) 20 ppm, (b) 70 ppm and (c) 140 ppm.

Habit plane of the hydride plates has also been determined in all the samples using single surface trace analysis method. These habit planes were found to lie close to and within 25° from the (0 0 0 1) plane of the α-phase.

4. Discussion

The microstructure of the Zr–1Nb alloy used in the present study is different from those observed in the other commonly used zirconium based alloys. Like Zr–2.5Nb, the Zr–1Nb alloy also has a two-phase microstructure consisting of the α and the β-phases. However, in these alloys the shape, size and size distributions of

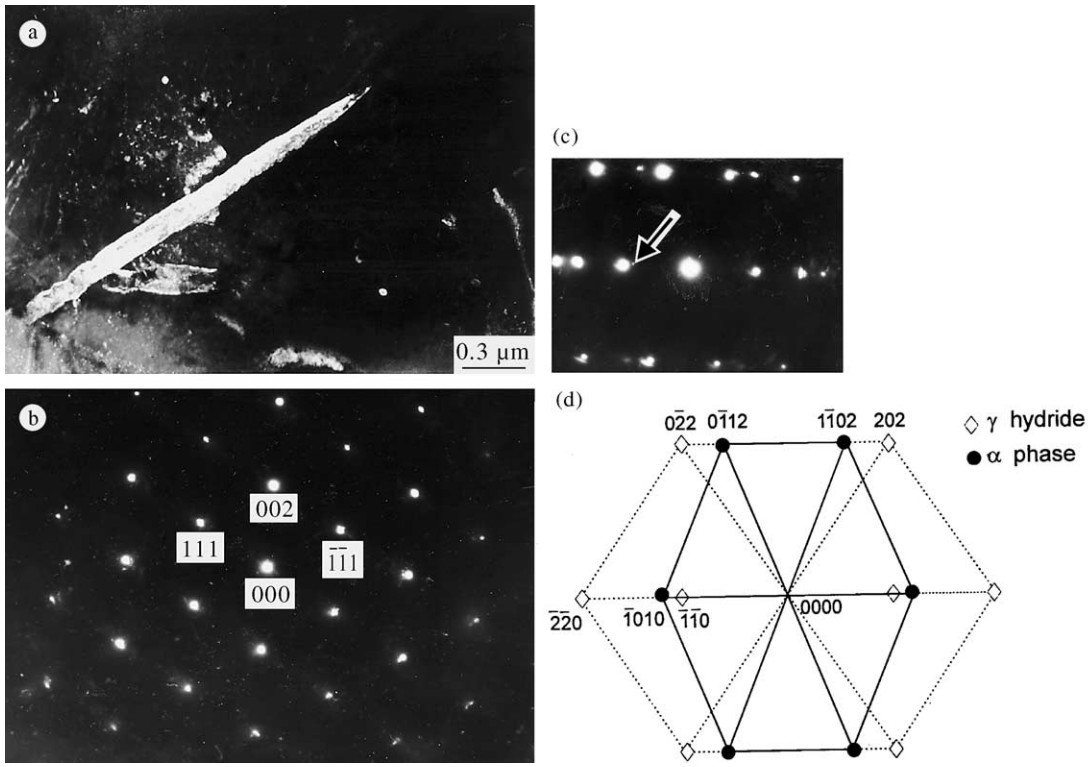

Fig. 5. (a) Dark field TEM micrograph showing the typical morphology of the γ-hydride plate. (b) SAED pattern obtained from the γ-hydride plate. Zone Axis = $[\bar{1}\,1\,0]$. (c) Composite SAED pattern showing reflections from α and γ-phases. Zone $\text{Axis}_{\alpha} = [\bar{2}\,4\,\bar{2}\,\bar{3}]$ and Zone $\text{Axis}_{\gamma} = [1\,\bar{1}\,\bar{1}]$. (d) Key to the SAED pattern shown in Fig. 5(c).

the β-phase are significantly different. The Zr–2.5Nb alloy has duplex microstructure in which the distribution of the α and the β-phases depends on the prior thermo-mechanical treatment. Whereas, in the Zr–1Nb alloy, as observed in this study, the β-phase is distributed as fine spherical particles within the α matrix. Zircaloys also have microstructure similar to the Zr–1Nb alloy but they essentially have a single phase microstructure in which intermetallic precipitates are distributed within the α matrix. In view of the above microstructural differences, it is important to study the hydride formation in this alloy and compare it with the hydride formation in other Zr base alloys.

In the present study hydride plates were found to lie in the axial circumferential plane. There are many factors such as texture [1,22], direction of working [7] and stress, grain boundary orientation [22] which govern the orientation of the habit plane of the hydride. It is known that the habit plane of the hydride plates lie close to the basal plane (0 0 0 1) of the α matrix [1,22]. In general, during the fabrication of zirconium alloy cladding tube large amount of compressive strain is given in the radial direction, which results in a material with predominantly radial basal pole texture and hence the hydrides lie in the axial circumferential plane. This situation is desirable since in the case of thin walled tube formation of radial hydrides would lead to the through-wall cracking of the tube.

The solubility of hydrogen in zirconium-based alloys is a strong function of temperature. The terminal solid solubility (TSS) of hydrogen in these alloys shows exponential dependence on temperature. Thus a small variation in hydrogen content in the alloy changes the TSS significantly. Northwood and Kosasih [1] has shown that TSS can be represented by an equation as follows:

$$\text{Cs (ppm)} = A\exp(-H/RT_s),$$

where Cs = terminal solubility, A = constant, ΔH = apparent difference between the partial molar heat of solution of hydrogen in the zirconium-alloy matrix and the hydride phase, R = gas constant, 8.314 $\text{J K}^{-1}\,\text{mol}^{-1}$. Using this equation TSS of hydrogen for the Zr–1Nb alloy used in the present study can be estimated. However, in absence of any data in literature for the Zr–1Nb alloy, values of constant estimated for the Zr–2.0Nb alloy have been used [25]. The temperatures corresponding to the TSS of 20, 70 and 140 ppm of hydrogen

in Zr–1Nb are estimated as 266, 343 and 396 °C respectively.

The diffusivity of hydrogen in zirconium can be expressed by the following equation as determined by Kearns [26]:

$$D = 0.217\exp(-8380/RT)\ \mathrm{mm^2\,s^{-1}},$$

where D = diffusivity of hydrogen in zirconium. Using this equation the diffusivity of hydrogen in zirconium at temperatures of 266, 343 and 396 °C are estimated as 33.45×10^{-3}, 42.25×10^{-3} and 48.1×10^{-3} $\mathrm{mm^2\,s^{-1}}$ respectively. Therefore, in alloys containing 140 ppm of hydrogen the precipitation of the hydride phase would start at relatively higher temperatures (~400°) where the diffusivity of hydrogen in the α matrix is high (48.53×10^{-3} $\mathrm{mm^2\,s^{-1}}$). In addition, matrix at these temperatures would be softer which can accommodate larger transformation strain associated with the hydride formation. Combined effect of these two would lead to the formation of larger size of hydride plates. This argument is supported by the fact that the larger hydride plates were encountered in samples containing 140 ppm of hydrogen as compared to samples containing lower content of hydrogen. Nucleation of hydride plates would occur continuously as the sample is cooled below the temperature at which the hydrogen content in the sample exceeds the TSS. In the case of higher hydrogen containing samples (140 ppm) the nucleation of hydride will occur over a larger temperature range. As discussed above, the size of these hydrides will depend on the temperature at which a particular hydride plate has nucleated. Thus it is expected that a larger size distribution will be observed in the samples containing higher hydrogen concentration.

In the present study two distinct morphologies of the δ-hydride has been observed; acicular morphology and zigzag morphology. The acicular morphology of δ-hydride plates has been reported in many earlier studies in other zirconium alloys [22]. As mentioned earlier this morphology of the hydride phase is due to the large transformation strain associated with the hydride formation. Therefore, the commonly observed acicular morphology of the hydride in the zirconium based alloys have been explained using Eshlby criteria which predicts that acicular (ellipsoidal) shape plates generates minimum elastic strain energy [27]. This situation is similar to the formation of martensite plates in the acicular shapes.

The other type of zigzag hydride morphology has not been commonly observed in the formation of δ-hydride in Zr base alloys. In the present case this morphology was seen in the samples containing larger concentration of hydrogen (140 ppm). In an earlier study Perovic et al. [22] have reported the formation of stacks of hydride plates in Zr–2.5Nb alloy loaded with 190 ppm of hydrogen. This zigzag hydride also appears to be a stack of very fine hydride plates. The individual plates in each stack are $\sim0.3\times0.06$ μm in size. The crystallographic analysis of this hydride showed that all the plates of a stack belong to a single variant of the hydride phase. It has been suggested in an earlier study that repeated nucleation and growth of plates sharing common habit plane results in formation of the stacks of hydride plates [8]. These stacks are generally constituted by more than one variant of hydrides in which the strain energy generated during transformation by one variant is compensated by the transformation strain energy of the other. However, in the present case the situation is somewhat different, as all the hydride plates of a stack belong to a single variant of the hydride phase. This difference in stacking behavior can be attributed to continuous cooling of samples during heat treatment A. Due to continuous cooling the equilibrium concentration of hydrogen in the α matrix is not attained at any given temperature. This results in the supersaturation of hydrogen in the matrix. At lower temperature when a hydride plate gets nucleated, matrix being stronger at that temperature would result in larger internal stresses at the hydride–matrix interface. The effect of this would lead to the followings:

(i) the growth of an individual plate would be limited to smaller size and
(ii) the diffusion of hydrogen would be preferred from lower stress regions (matrix) to higher stress region (interface) resulting in the nucleation of a new hydride plate sharing the common hydride habit plane.

The nucleation of hydride plates in such a fashion would continue till all the hydrogen from the supersaturated matrix is consumed giving rise to stack of hydride plates with zigzag morphology. The presence of internal stresses in the formation of zigzag morphology therefore appears to be a necessary condition. In order to support the above viewpoint evidences of the presence of internal stresses during hydride precipitation have been examined critically. A closer examination has revealed that the orientation of the stack of hydride plates is changing as it is progressing. This change in orientation of the hydride can be correlated to the internal stresses generated in the system. As it is known that under internal stress hydride plate reorient themselves, it can be envisaged that under the influence of stresses generated during precipitation of the hydride the growing plates reorient their habit plane to attain the least energy configuration. This observation is in agreement with that observed by Perovic et al. [22]. The sympathetic nucleation of the stack of hydride plates with elastic strain accommodation in the matrix is responsible for the large size of the δ-hydride colony with zigzag morphology.

It is shown in several studies that on rapidly cooling hydrogen-containing samples, the formation of

metastable γ-hydride phase is preferred over the δ-hydride [28–31]. The formation of the γ-hydride phase is of particular interest since it may form at lower temperatures where the rate of self-diffusion of zirconium is not significant and hence it has been suggested that hydrides must form by a displacive or martensitic transformation [32]. In support of the above hypothesis, a study by Carpenter has shown electron diffraction contrast effects at γ-hydride needles formed in rapidly cooled zirconium suggesting a shear transformation [33]. In Zr–20Nb and Zr–2.5Nb alloys the observation of acicular or needle like morphology and internally twinned γ-hydride plate are typical characteristics of martensitic transformation [24,32]. The phenomenological theory of martensite has accurately predicted the habit plane of the hydride plate in a β to γ transformation [34]. It has also been suggested that the α to γ transformation involves shearing process in which firstly hydrogen rich regions in α-phase transforms to β-phase following Burgers relationship and subsequently β transforms to γ martensitically [32].

In the present investigation predominantly fine needle like γ-hydride plates were observed. However these plates were not showing any internally twinned structure like those observed in the hydrides of Zr–2.5Nb alloy. This situation is analogues to martensite formation in Zr–1Nb and Zr–2.5Nb alloys where internally twinned martensite is observed in the case of later only. This is due to the fact that twinning is preferred as the lattice invariant shear (LIS) in the case of Zr–2.5Nb martensite formation [35]. Similarly the above logic may be extended for the absence of internally twinned γ-hydride plates in the Zr–1Nb alloy. Bradbrook et al. [29] have reported a similar kind of observation in zirconium and Zircaloy-2 where specimens rapidly quenched to room temperature contained only untwined γ-hydrides.

The absence of macroscopic stack of hydride plates in γ-hydride formation may be attributed to smaller volume change associated with formation of γ-hydride plates $[(V_\gamma - V_\alpha) \sim 12.3\%; (V_\delta - V_\alpha)] \sim 17.2\%$ [4]. Thus stresses generated in the α matrix may not be sufficient for sympathetic nucleation to occur and give rise to stack of hydride plates. In addition to that γ-hydride forms at lower temperature where the diffusivity of hydrogen is expected to be low enough to cause the migration of hydrogen in the high stress (where first hydride has formed) regions. Besides, γ-hydride forms under the condition of quenching from the dissolution temperature, which generally gives rise to a finer dispersion of precipitates in the matrix phase.

In this study it has been seen that the hydride plates were cutting across adjacent α grains and β precipitates i.e., in other words a γ-hydride plate disregards the α/α and α/β interface. In an earlier study Dey et al. [32] have brought out the similarities in the structures of the α, β and the γ-hydride phases. That may be the possible reason for formation of the γ-hydride phase in the α-phase as well as in the β-phase of Zr and of hydride plates ignoring the α/α and α/β interface.

The orientation relationship observed in the present study between the α matrix and the γ-hydride phase as well as between the α matrix and the δ-hydride phase has been found to be similar to those observed in other Zr base alloys [1,8,22,24]. This is due to the similarity in the structure of the various phases formed in the Zr–1Nb alloy and other Zr base alloys. Observations of similar morphology and orientation relationship between various phases indicate that the underlying mechanism of hydride formation is same. However, subtle differences like deviation in the habit plane orientation of the hydride phase with respect to the basal plane pole is much larger than those observed in Zr and other Zr base alloys [8,22,24].

5. Conclusions

The conclusions drawn from the present study can be summarized as follows:

(1) The microstructure of the Zr–1Nb alloy comprised two-phase microstructure in which fine, spherical particles of the β-phase were uniformly distributed in the α matrix.
(2) Two different morphologies of the δ-hydride phase have been observed when samples of the Zr–1Nb alloy containing 20, 70 and 140 ppm were slowly cooled from 400 °C. The acicular morphology was noticed in all the samples whereas the zigzag morphology was noticed in samples containing higher concentration of hydrogen.
(3) The formation of the γ-hydride phase was observed in hydrogen charged samples of the Zr–1Nb alloy, which are rapidly cooled from 400 °C. The morphology of the γ-hydride phase remained acicular in all the samples. Unlike the Zr–2.5Nb alloy, internally twinned hydride plates were not observed in the Zr–1Nb alloy.
(4) The orientation relationships between the α and the δ-hydride phase and between the α and the γ-hydride phase were found to be the same as those observed in the case of other Zr base alloys. However, in the Zr–1Nb alloy, deviation of the habit planes from the basal plane pole in both types of hydride phases were found to be larger than the deviation observed in Zr and other Zr base alloys.

Acknowledgements

The authors wish to thank Dr C. Ganguly, Chief Executive, Nuclear Fuels Complex, Hyderabad and his colleagues for supplying samples and for continuous

exchange of information. The help and encouragement received during the course of this study form Dr P.K. De, Head, Materials Science Division, Bhabha Atomic Research Centre is gratefully acknowledged.

References

[1] D.O. Northwood, U. Kosasih, Int. Metals Rev. 28 (1983) 92.
[2] J.J. Kearns, J. Nucl. Mater. 22 (1967) 292.
[3] I. Aitchison, Applications-Related Phenomena in Zirconium and Its Alloys, in: STP 458, ASTM, Philadelphia, PA, 1969, p. 160.
[4] R.J. Beck, ASM Trans. Q. 55 (1962) 546.
[5] E.J. Goon, J. Malgiolio, USAEC Report NYO-7547, 1958.
[6] C.E. Coleman, D. Hardie, J. Less-Common Met. 11 (1966) 168.
[7] C.E. Ells, J. Nucl. Mater. 28 (1968) 129.
[8] V. Perovic, G.C. Weatherly, J. Nucl. Mater. 126 (1984) 160.
[9] R. Tricot, Rev. Gen. Nucl. (January–February) (1990) 8.
[10] C. Lemaignan, A.T. Motta, Zirconium alloys in nuclear applications, in: R.W. Cahn, P. Hassen, E.J. Kramer (Eds.), Nuclear Materials, Materials Science and Technology, A Comprehensive Treatment, 10B, VCH Verlagsgesellschaft mbH, Weinheim, 1994 (Chapter 7).
[11] D.L. Douglass, The Metallurgy of Zirconium, Int. Atomic Energy Agency, Vienna, 1971.
[12] B.A. Cheadle, C.E. Coleman, H. Licht, Nucl. Technol. 57 (1982) 413.
[13] T.R.G. Kutty, K. Ravi, C. Ganguly, J. Nucl. Mater. 265 (1999) 91.
[14] V.F. Urbanic, B. Cox, Can. Metall. Q. 24 (3) (1985) 189.
[15] G.P. Sabol, G.R. Kilp, M.G. Balfour, E. Roberts, in: ASTM-STP-1023, ASTM, Philadelphia, 1989, p. 227.
[16] S.L. Wadekar, S. Ganguly, G.K. Dey, J.K. Chakravarthy, V. Chopra, P. Pande, in: S. Banerjee, R. Ramanujam (Eds.), Proceedings of International Conference on Physical Metallurgy (ICPM-94), Bombay, India, 9–11 March 1994, Gordon and Breach, Amsterdam, 1996, p. 443.
[17] K. Balaramamurthy, in: Proceedings of Zirconium Alloys for Reactor Components (ZARC-91), Bombay, India, 1991, Department of Atomic Energy, Bombay, 1991, p. K-1.
[18] C.E. Coleman, J.F.R. Ambler, Annual Volume, Metallurgical Society of CIM, Montreal, PQ, 1978, p. 81.
[19] V. Perovic, G.C. Weatherly, S.R. MacEwen, M. Leger, Acta Metall. 40 (1992) 363.
[20] A.R. Daniel, Terminal solid solubility of hydrogen in Zircaloy-2, Report AECL-2453, Atomic Energy of Canada Ltd., 1966.
[21] D. Srivastava, G.K. Dey, S. Banerjee, Metall. Mater. Trans. A 26A (1995) 2707.
[22] V. Perovic, G.C. Weatherly, C.J. Simpson, Acta Metall. 31 (1983) 1381.
[23] C.D. Cann, M.P. Puls, E.E. Sexton, W.G. Hutchings, J. Nucl. Mater. 126 (1984) 197.
[24] G.C. Weatherly, Acta Metall. 29 (1981) 501.
[25] W.H. Erickson, D. Hardie, J. Nucl. Mater. 18 (1964) 254.
[26] J.J. Kearns, J. Nucl. Mater. 27 (1968) 64.
[27] J.D. Eshelby, Proc. R. Soc. London, A 241 (1957) 376.
[28] J.E. Bailey, Acta Metall. 11 (1963) 267.
[29] J.S. Bradbrook, G.W. Lorimer, N. Ridley, J. Nucl. Mater. 42 (1972) 142.
[30] B.J. Gill, P. Cotterill, J.E. Bailey, J. Less-Common Met. 39 (1975) 189.
[31] B.J. Gill, J.E. Bailey, P. Cotterill, J. Less-Common Met. 40 (1975) 129.
[32] G.K. Dey, S. Banerjee, P. Mukhopadhyay, J. Phys. Fr. C 4 (1982) 327.
[33] G.J.C. Carpenter, Acta Metall. 26 (1978) 1225.
[34] D. Srivastava, Beta phase transformations in zirconium base alloys, PhD thesis, Indian Institute of Science, Bangalore, India, July 1996.
[35] Z. Nishiyama, in: M.E. Fine, M. Meshii, C.M. Wayman (Eds.), Material Science Series, Academic Press, New York, 1988.